Hydrothermal synthesized urchin-like nickel-cobalt carbonate hollow spheres for sensitive amperometric detection of nitrite

Article *in* Journal of Alloys and Compounds · June 2017

DOI: 10.1016/j.jallcom.2017.03.059

Shun Lu
Faculty of Materials and Energy
4 PUBLICATIONS **1** CITATION
SEE PROFILE

Chi Yang
Nanjing University of Information Science & …
36 PUBLICATIONS **324** CITATIONS
SEE PROFILE

Journal of Alloys and Compounds 708 (2017) 780–786

Contents lists available at ScienceDirect

Journal of Alloys and Compounds

journal homepage: http://www.elsevier.com/locate/jalcom

Hydrothermal synthesized urchin-like nickel-cobalt carbonate hollow spheres for sensitive amperometric detection of nitrite

Shun Lu [a, b], Chi Yang [a, *], Ming Nie [b, **]

[a] *Yale-NUIST Center on Atmospheric Environment, Nanjing University of Information Science and Technology, Nanjing 210044, China*
[b] *Faculty of Materials and Energy, Southwest University, Chongqing 400715, China*

A R T I C L E I N F O

Article history:
Received 6 February 2017
Received in revised form
1 March 2017
Accepted 6 March 2017
Available online 8 March 2017

Keywords:
Urchin-like
Nickel-cobalt carbonate
Electrochemical sensor
Nitrite

A B S T R A C T

In this article, we present a facile and low-cost method to prepare urchin-like nickel-cobalt carbonate hollow spheres that display excellent electrooxidation of nitrite. The as-fabricated samples are characterized by XRD, SEM, TGA, and BET. The results confirm that the successful formation of nickel carbonate and cobalt carbonate at ratio of 1/2, and their entirely uniform hollow microspherical structure with an average pore size of 4 nm and a pore volume of 0.15 $cm^3\ g^{-1}$. Moreover, the as-prepared nitrite sensor has a good electrochemical response with the linear range of 5–4000 μM and the detection limit of 0.002 μM under optimum conditions, respectively with the correlation coefficient of 0.999. The fabricated nitrite sensor also exhibited high sensitivity and good stability.

1. Introduction

Growing concern worldwide about environmental pollution and its effect on the air quality, food safety and human health, environment problems had attracted much attention in the past decades [1,2]. Unlike several other global problems such as greenhouse effect and soil erosion, ubiquitous urban smog (PM 2.5, particulate matter less than 2.5 μM) has rapidly ascended to hot topic mostly due to soaring public outcries and extensive media coverages while related research discourse clearly lags behind. On average, PM 2.5 is majorly composed of organic matters, sulfate, nitrate and ammonium in Beijing [3], Although the detailed effects of each type of PM on health have not yet been established, recent studies have identified a strong exposure–response relationship between PM and both short-term and long-term health effects [4]. Therefore, monitoring air, soil and water for hazardous pollutants is important and based on the need to protect the environment and public health from potential pollutants.

Nitrite, an intermediate product in the nitrogen cycle, is also one of the most common pollutants in aquatic environment [5]. The importance of nitrite stems from its effects on human health, and nitrite can become poisonous at high concentrations to animals and human beings because it probably results in generation of carcinogenic nitrosamines [6]. Nitrous acid may dissociate in to OH^- and NO^+. The latter radical oxidizes the Fe^{2+} of the hemoglobin to Fe^{3+}, which in oxidized form is unable to adsorb O_2 [7]. Therefore, the detection of nitrite (NO_2^-) is of great importance. Additionally, nitrite is widely used as a preservative, dyeing agent, fertilizer and food additive [8,9]. Nitrite is also important in biochemistry as a source of the potent vasodilator nitric oxide [10]. Therefore, a variety of techniques have been developed for the detection and monitoring of nitrite, such as chromatography, chemiluminescence, capillary electrophoresis, spectrophotometry and electrochemical methods [11–15]. Among them, electrochemical techniques are preferred because of their rapid response, relatively low cost, high sensitivity, time saving, and good selectivity [15,16].

Generally, the electrochemical methods for detection of nitrite, can be divided into two distinct types: (1) oxidation, and (2) reduction, of nitrite on different electrodes [10]. Anodic oxidation of nitrite is preferred with the final product of nitrate (NO_3^-), due to several by-products depending on electrode condition and property of catalysts affecting reduction of nitrite on cathode [17,18]. However, the electrooxidation of nitrite has some drawbacks, sluggish electron transfer kinetics included. Additionally, the oxidation of nitrite on these conventional solid electrodes, still suffers large overpotentials, causes surface oxide formation as well as fouling effects, and decreases the selectivity and accuracy by

---

* Corresponding author.
** Corresponding author.
E-mail addresses: yangchi@seu.edu.cn (C. Yang), niemingcqu@126.com (M. Nie).

http://dx.doi.org/10.1016/j.jallcom.2017.03.059
0925-8388/

other electroactive interferences [18]. In order to circumvent these inherent difficulties, the surface of bare electrodes is being modified with suitable catalysts to increase interfacial electron transfer and decrease the oxidation potential [9].

Recently, nano/micro devices fabricated by nanometer-sized building blocks have been regarded as promising electrocatalysts toward energy storage and conversion, such as oxygen reduction reaction (ORR), oxygen evolution reaction (OER), and electrochemical capacitors (ECs) due to their nano/micro-scale second blocks and large active sites density [19–22]. Particularly, spinel nickel cobaltite ($NiCo_2O_4$), as one of mixed metal compounds, has recently attracted growing interests, because of its different morphologies and electrochemical applications [23]. Generally, the spinel $NiCo_2O_4$ is made up of Ni^{2+}, Co^{2+}, and urea via hydrothermal treatment and thermal decomposition [24,25]. Among those procedures, we accidently discovered its intermediate product, nickel-cobalt carbonate, which possesses novel structures and morphologies [26,27]. To the best of our knowledge, nickel and cobalt-based oxides, layered double hydroxides, and metal-organic frameworks have attracted much attention because of their potentially high activity and relatively easy operation, however, nickel-cobalt carbonate (here, denoted as NC) with novel properties has been rarely studied in electrochemical detection [24,26,28,29]. Previous literature, which based on their nano/micro-structure and characterized via microscopy techniques, were reported to detect nitrite, especially for porous materials. Mesopores are supposed to facilitate the diffusion of reactants in the electrocatalytic process and increase the number of available active sites [23]. Therefore, BET test was applied to analysis its structure information.

Herein, we present a facile and low-cost method to prepare urchin-like NC hollow spheres that display excellent electro-oxidation of nitrite. The as-obtained hollow spheres have entirely uniform microspherical structure with an average pore size of 4 nm and a pore volume of 0.15 $cm^3\ g^{-1}$, which would facilitate reactant transport inside the pores, assuring better contact the catalyst and better stability. The as-synthesized sensor shows good electrochemical response to nitrite and offers a new platform for designing sensors to detect nitrite sensitively and selectively.

2. Experimental

2.1. Materials

$Ni(NO_3)_2 \cdot 6H_2O$ and $Co(NO_3)_2 \cdot 6H_2O$ were bought from Sigma–Aldrich (China) Co., Ltd. Sodium nitrite ($NaNO_2$) was purchased from Sinopharm Chemical Reagent Co., Ltd. Phosphate buffered solution (PBS, 0.1 M) containing 0.15 M NaCl was prepared by mixing different proportions of NaH_2PO_4 and Na_2HPO_4, and then the pH adjusted with 0.1 M NaOH and H_3PO_4. Deionized water was used for preparation of aqueous solution, and all the chemicals used in this study were analytical grade and were used without further purification.

2.2. Preparation of $NiCo_2CO_3(OH)_2$ hollow spheres

In a typical synthesis, 40.0 g $CO(NH_2)_2$ was dissolved in 75 mL deionized water with assistance of ultrasonic vibration, followed by rapid addition of 25 mL 1.46 g $Ni(NO_3)_2 \cdot 6H_2O$ and 2.91 g $Co(NO_3)_2 \cdot 6H_2O$ aqueous solution. The mixture was dealt with ultrasonic for 30 min at room temperature, then the solution was transferred to a Teflon-lined stainless steel autoclave and heated in an oven at 90 °C for 6 h. The precipitates were dried at 65 °C for 6 h in a vacuum oven, then collected by centrifugal filtration, washed with deionized water and absolute ethanol to obtain the $NiCo_2CO_3(OH)_2$ materials.

2.3. Characterization

To evaluate the crystalline structure of the as-obtained NC, X-ray diffraction measurements were carried out on a D/Max-III (XRD, Rigaku Co. Ltd., Japan) using Cu Kα radiation $\lambda = 0.15406$ nm at a scanning rate of 5°/min and operated at 34 kV and 26 mA. The morphologies were observed by field emission scanning electron microscopy (FESEM, Hitachi S4800, Japan) and constituent content was analyzed by energy-dispersive X-ray spectroscopy (EDS, Oxford Co. Ltd., England). Transmission electron microscopy investigations were carried out on TEM JEM-2010HR at 200 kV (TEM, JEOL, Japan), the corresponding selected area electron diffraction (SAED) and high resolution TEM (HRTEM) were used to characterize the morphology and structure. Thermogravimetric analysis (TGA) was conducted by an integrated thermal analyzer (STA 449C) with a heating speed of 10 °C/min in air. The Brunauer–Emmett–Teller specific surface area (BET) of the sample was characterized by analysis of the N_2 adsorption–desorption isotherms, performed at 77 K with Micromeritics ASAP 2020 sorption analyzer in a relative pressure (P/P_0) range from 10^{-6} to 1 after degassing the samples at 200 °C for 3 h.

2.4. Electrochemical characterization

Electrochemical studies were carried out in a standard three-electrode system controlled by electrochemical workstation (CHI 630D, Chenhua Ltd, Co. China). A glassy carbon electrode (GCE, 4 mm in diameter) was polished carefully on felt pads with 1.0, 0.3 and 0.05 μm alumina slurry in turn and cleaned by brief sonication in ethanol and water until a mirror-like surface was formed. A defined amount of NC (2.0 mg) were suspended in 2 mL ethanol and ultrasonicated for 30 min. Then a drop of the suspension (1.0 mg/mL, 4.0 μL) was coated on the surface of freshly polished GCE, then casted with nafion (wt. 5.0%, 4.0 μL) and dried in an inverted beaker at room temperature. The mass loading of active materials was about 0.03 mg cm^{-2}. The as-prepared NC spheres modified on GCE (denoted as NCE), a platinum foil, and a saturated calomel electrode (SCE) were used as the working electrode, counter electrode, and reference electrode, respectively. The electrochemical performances were examined by cyclic voltammetry (CV) and amperometric response (i-t). The electrolytes for tests were 0.1 M PBS. All the tests were carried out at room temperature (about 25 °C).

3. Results and discussion

NC hollow spheres, which are mixed metal carbonate salts, were fabricated by reacting metal cations (Ni^{2+} and Co^{2+}) with CO_3^{2-} and OH^- anions slowly released from the hydrolysis of urea during the hydrothermal process, as illustrated in Scheme 1.

X-ray diffraction is employed to characterize the crystal structure of sample. Fig. 1a depicts the typical Powder XRD pattern of the NC sample. By comparing the peak positions with the standard PDF cards, it is easy to found that this compound is composed of two phase: $NiCO_3(OH)_2 \cdot 2H_2O$ (PDF #29-0868) and $Co(CO_3)_{0.5}(OH)_2 \cdot 0.11H_2O$ (PDF #48-0083), rather not $NiCo_2O_4$ (PDF #20-0781). Fig. 1b–d demonstrates the FESEM images with different magnifications for NC hollow spheres.

Urchin-like microspheres with a size of ~3.5 μm can be found clearly in Fig. 1b, and the surface of these spherical structures is fixed with many nanowires (NWs) with sharp tips in a radial form, they take on an urchin-like appearance as a whole. Hollow structures also can be confirmed (Fig. 1c). The as-obtained NC hollow sphere also entirely consists of uniform micro spherical structure without the size change, but spheres aggression in part area may

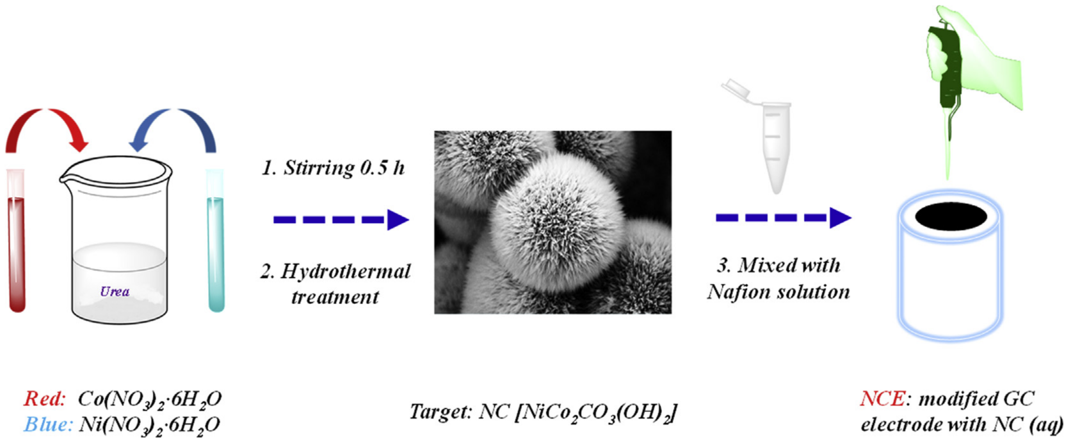

Scheme 1. Preparation of urchin-like NC hollow sphere and its modified electrode (NCE).

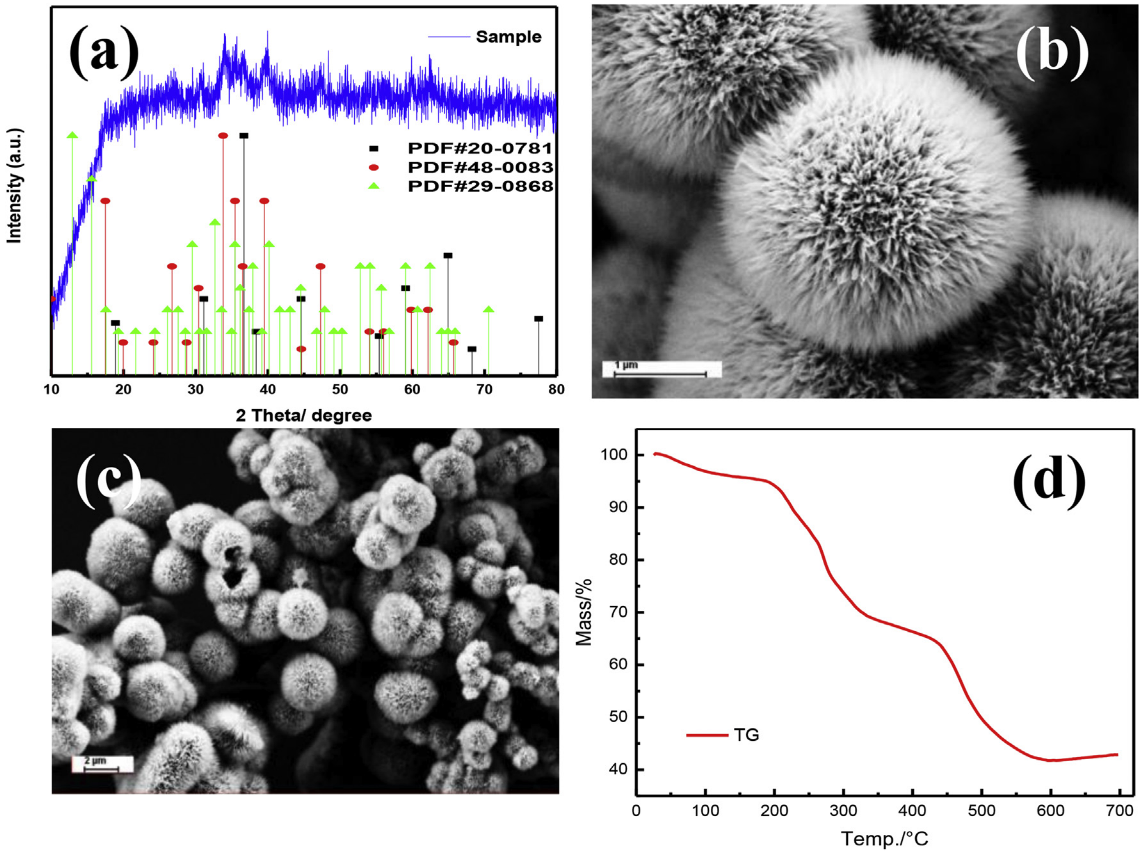

Fig. 1. Powder XRD patterns (a), different magnification SEM images (b, c) and thermogravimetric curve (d) of NC hollow spheres.

result of decreasing the amount of active sites. Fig. 1d displays TGA curves of NC hollow spheres in the temperature range of 20–700 °C, which depict three different decomposition modes for the various carbonate species produced from NC hollow spheres. The TGA curve showed a total weight loss of ~60% in the given temperature range. Water loss of around 8% was observed until 200 °C and the sum of CO_2 weight loss arrived ~50% until 600 °C, which can be ascribed the decomposition of carbonates that cobalt and nickel carbonate included.

Fig. 2a describes the element mapping results for the distributions of Ni and Co homogeneously based on an individual NC hollow sphere. To further confirm the composition of the NC product, EDS was conducted. Ni, Co, C, and O elements were detected (Fig. 2b), and the contents of Ni and Co were determined to be 6.51 and 13.34%, respectively. The atom ratio of Ni to Co is close to 1: 2, in good agreement with the stoichiometric ratio of Ni/Co in $NiCo_2CO_3(OH)_2$ hollow spheres.

The NC hollow spheres have a large surface area of ~101.54 m^2 g^{-1} with a type-IV isotherm measured by the BET method [30]. The distinct hysteresis loop at a relative pressure of above 0.5–0.8 reflects the capillary condensation of mesopores, as presented in Fig. 3a. The mesoporous structure has an average pore

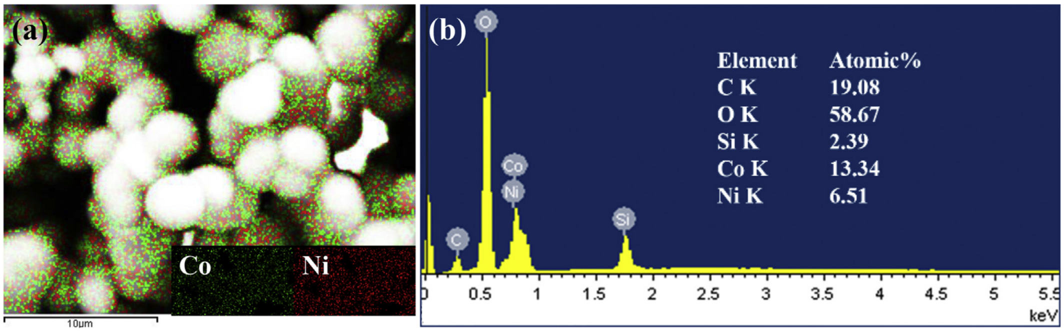

Fig. 2. Element mapping (a) and EDS (b) of urchin-like NC hollow spheres.

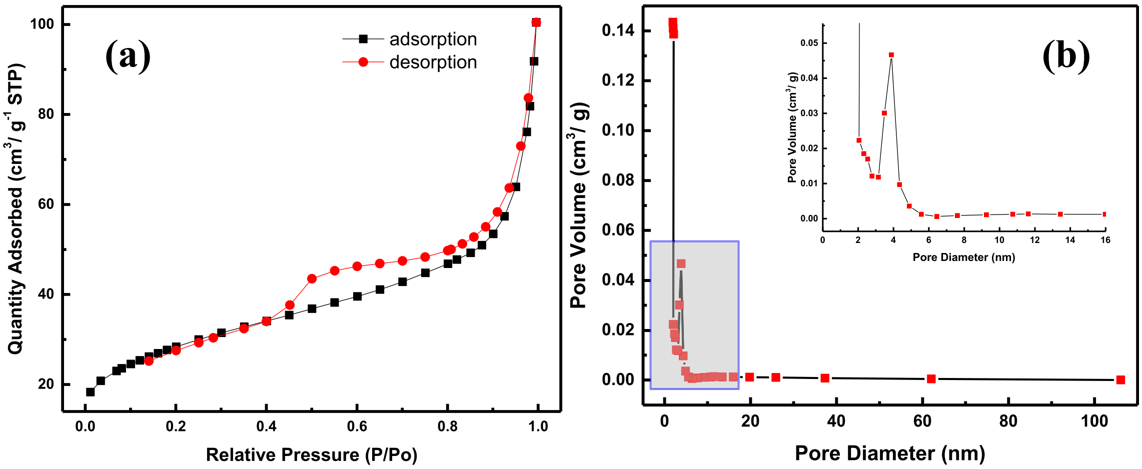

Fig. 3. Nitrogen adsorption and desorption isotherm (a) and the corresponding BJH pore size distribution curve (b) of the urchin-like NC hollow spheres.

size of 4 nm and a pore volume of 0.15 cm^3 g^{-1}, as verified by the Barrett-Joyner-Halenda (BJH) method (inset of Fig. 3b). The mesoporous structure can be ascribed to the successive release and loss of CO_2 and H_2O during the hydrothermal treatment of the $NiCo_2(OH)_{3y}(CO_3)_{1.5(2-y)}\cdot nH_2O$ precursor [31].

TEM analysis was performed to examine the crystal orientations and growth directions of urchin-like NC hollow spheres. It is found that NC hollow spheres are assembled by many nanospikes (Fig. 4a and b). HRTEM analysis provides more detailed structural information about the fine crystal structures (Fig. 4c). The clear lattice fringes of NC, revealing their good crystallization. The distance of the interplanar distance between adjacent lattice spacing is *ca.* 0.23 nm, which is consistent with the (1 1 1) planes of the face-centered-cubic (fcc) NC hollow spheres. This observation indicates that NC hollow spheres preferentially grow along the (1 1 1) directions in the present synthesis, although different orientations of the lattice fringes are detected from other nanospikes. Additionally, their polycrystalline structures are clearly demonstrated by the respective SAED pattern taken from urchin-like NC hollow spheres (Fig. 4d).

In order to evaluate the potential application of NC hollow spheres, electrochemical sensors for nitrite detection are fabricated by dropping the dispersion solution with NC hollow spheres on surface of GCE. Fig. 5a is the typical CV curves, showing the CVs of bare GCE (dark cyan line) and NCE (red line) towards the oxidation of 5.0 mM nitrite, meanwhile, bare GCE (black line) and NCE (blue line) also are observed in the absence of nitrite. In the potential range of 0.2–1.2 V, bare GCE (black line) does not show any redox peak. In contrast, a dramatic change in the CV curve is observed with the NCE (red line), especially around 0.9 V, which is corresponded to the oxidation of nitrite.

The plot of Fig. 5b demonstrates the influence of pH (in the range of 5.4–8.0) on the anodic peak current response. The results show that the peak current increases rapidly with increasing pH and reaches a maximum at pH 7.0. Further increasing pH to 8.0 decreases the current response. This result is well in accordance with previous reports [9,32]. The cause of relatively low current response at acidic medium may be due to the disporportionation of NO_2^- to NO and NO_3^-. On the other hand, the lack of proton at higher pH conditions will also affect the current response because the oxidation of nitrite is a proton dependent process. Moreover, some oxidation products formed at the electrode surface under high pH conditions would also inhibit the oxidation process. Therefore, pH 7.0 was selected as the optimal pH. The charge transfer properties of NCE were characterized by the electrochemical method. As depicted in Fig. 5c, the obtained CVs at the bare GCE (black line) and NCE (red line) in the 5 mM $K_3[Fe(CN)_6]$ and 0.1 M KCl solution at 50 mV s^{-1}. A pair of redox peaks was observed in each CV, which was ascribed to the redox of $[Fe(CN)_6]^{3+}$. After being modified with NC, the anodic peak and cathodic peak (red line) both increased because of the good electrical conductivity and large specific surface area of NC [26,33].

The effect of scan rate (ν) on the oxidation of nitrite has been performed at NCE from 20 to 200 mV s^{-1} in PBS (0.1 M, pH 7.0) containing 5.0 mM nitrite. Fig. 6a depicts the relationship between scan rate and anodic current response of nitrite oxidation. It is noted that the oxidation potential of nitrite gradually shifts to the positive potential when the scan rate increases. The results show

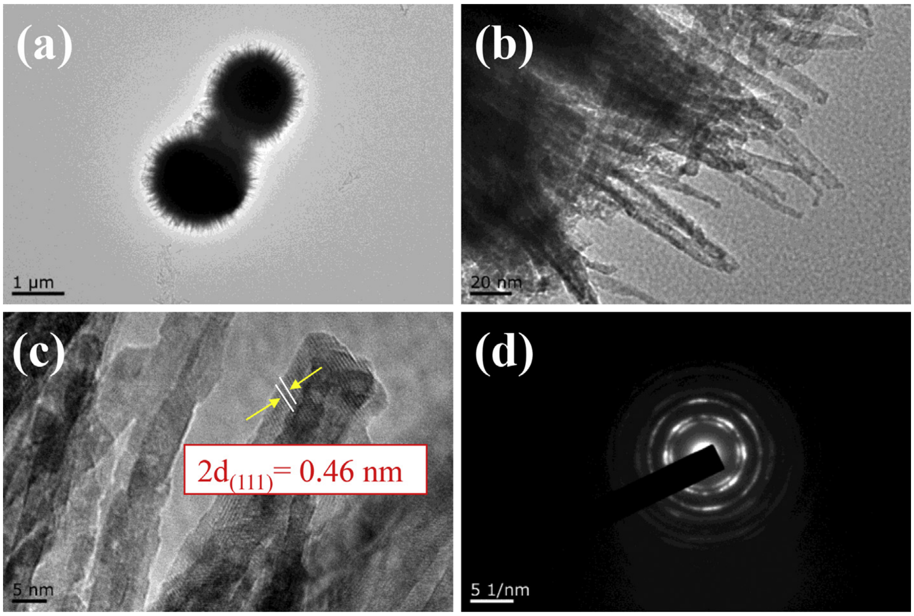

Fig. 4. TEM (a and b) and HRTEM image (c), SAED pattern (d) of NC hollow spheres.

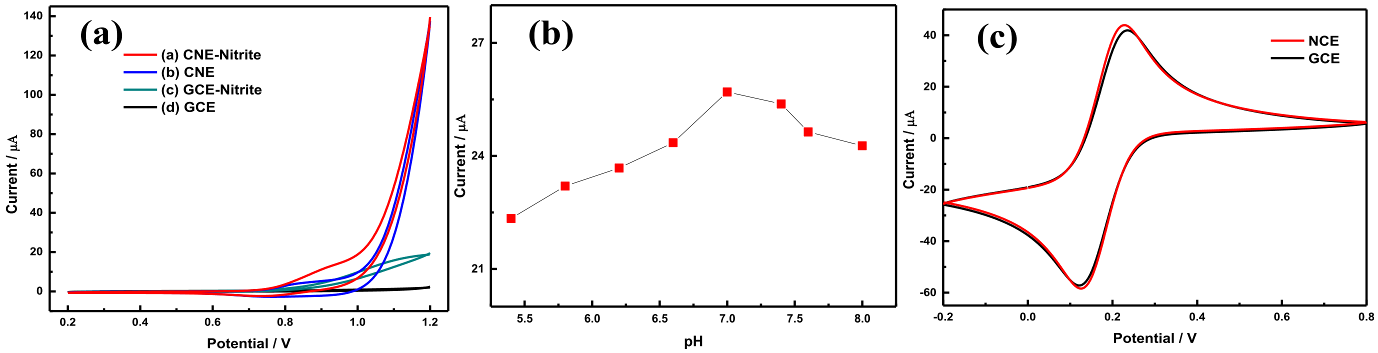

Fig. 5. (a) CVs on the bare GCE (black line), NCE (blue line) in 0.1 M PBS (pH 7.0) and bare GCE (dark cyan line), NCE (red line) in 0.1 M PBS (pH 7.0) with 5.0 mM nitrite solution, (b) The effect of pH on the current response of 5.0 mM nitrite at NCE, (c) CVs of the bare GCE (black line), and NCE (red line) in the 5 mM $K_3[Fe(CN)_6]$/0.1 M KCl solution. Scan rate: 50 mV s^{-1}. (For interpretation of the references to colour in this figure legend, the reader is referred to the web version of this article.)

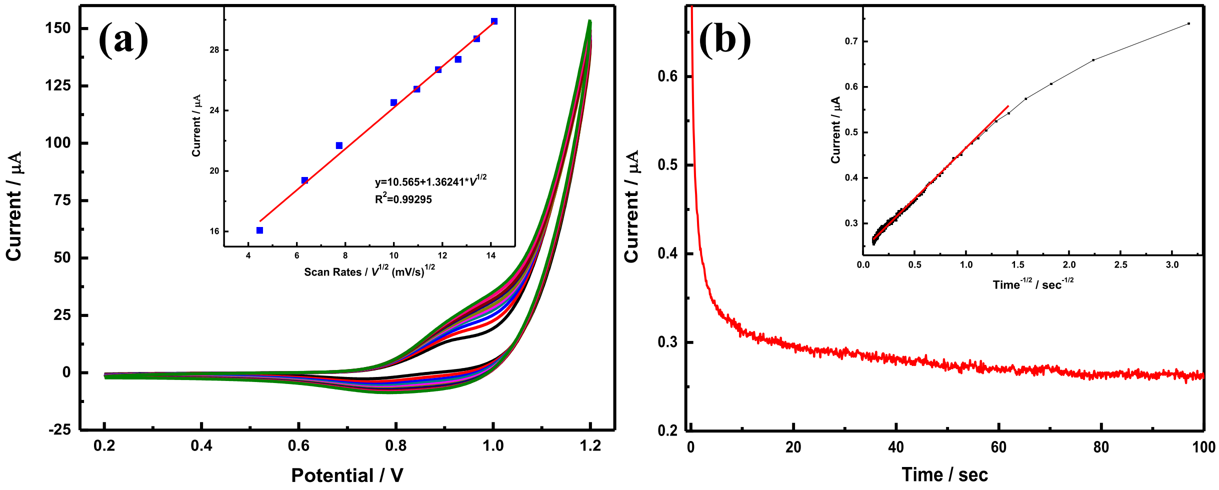

Fig. 6. (a) CVs of nitrite (5.0 mM) on NCE in PBS (0.1 M, pH 7.0) at different scan rates (20–200 mV s^{-1}), inset: the plot of peak current *vs.* square root of scan rates, (b) Amperometric response of NCE in 0.1 M PBS (pH 7.0) with 0.1 mM of nitrite solution at potential of 0.90 V, inset: the plot of *I vs.* $t^{-1/2}$ derived from the amperometric *i*-*t* curve.

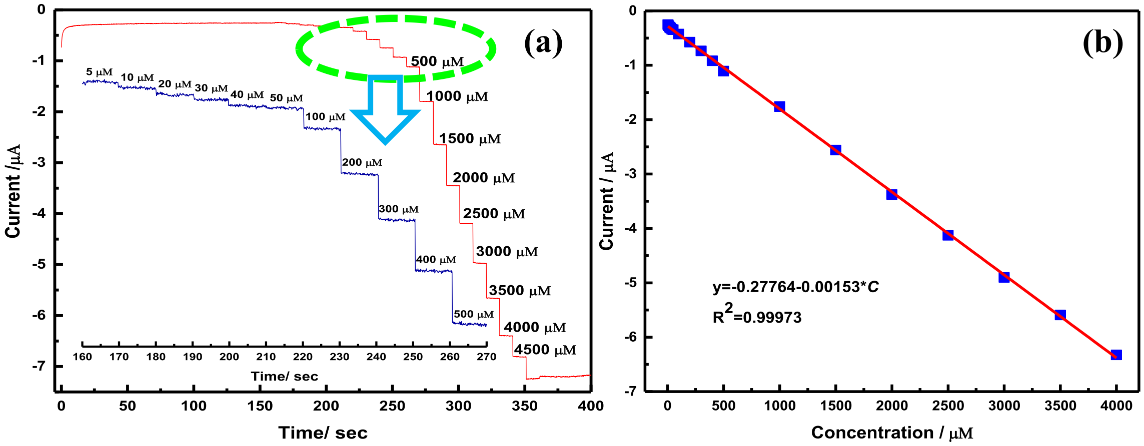

Fig. 7. (a) Amperometric responses of nitrite on NCE upon successive addition of nitrite to 0.1 M PBS (pH 7.0) by applying a constant potential of 0.9 V. (b) the plot of current *vs.* nitrite concentration.

Table 1
Comparison of NCE with other sensors for nitrite detection.

Electrode materials	Methods	Linear range/μM	LOD/μM	Ref.
Au [a]NPs/[b]Ch	[c]DPV	0.4–750	0.1	[35]
Fe_2O_3 NPs/rGO	DPV	0.05–780	0.015	[16]
β-MnO_2	Amperometric	0.29–26090	0.29	[36]
Au–Pd/rGO	Amperometric	0.05–1000	0.02	[37]
Au NPs/[d]MWCPE	[e]SWV	0.05–250	0.01	[38]
Ag nanoplates	Amperometric	10–1000	1.2	[39]
NC	Amperometric	5–4000	0.002	This work

[a] Nanoparticles.
[b] Choline chloride (Ch).
[c] Differential Pulse Voltammetry.
[d] Multi-walled carbon nanotube/carbon paste electrode.
[e] Square Wave Voltammograms.

that the oxidation current of nitrite is proportional to the square root of scan rate (the inset of Fig. 6a). The linear regression equation for the anodic peak current is $y = 10.565 + 1.36241*\nu^{1/2}$; $R^2 = 0.99295$. Good linear relationship obtained between $\nu^{1/2}$ and I_{pa} confirmed that the oxidation process is diffusion-controlled. Remarkably, the nitrite oxidation is a second-order homogeneous disporportionation process and the mechanism of the oxidation can be expressed as Eq. (1) [34].

$$NO_2^- + H_2O \rightarrow NO_3^- + 2H^+ + 2e^- \quad (1)$$

Fig. 6b depicts the amperometric response of NCE in 0.1 mM of nitrite solution when a potential of 0.9 V was applied. A straight line plot of the current against minus square root of time was deduced, as depicts in the inset of Fig. 6b, further confirming that the oxidation of nitrite is a typical diffusion controlled process.

Fig. 7a shows the amperometric *i*–*t* curve obtained at NCE upon successive addition of nitrite at the applied potential of 0.9 V. The linear response range of the biosensor was from 5 to 4000 μM with a regression coefficient of 0.999 (n = 19) and a sensitivity of 1.21×10^{-4} μA μM^{-1} cm^{-2}, and the detection limit (LOD) was estimated to be 0.002 μM (a signal to noise ratio of 3) (Fig. 7b). Performances of various nitrite biosensors are listed in Table 1. It is clear that the performance of NCE was significantly improved. The important analytical parameters such as test technique, linear range, and LOD of the sensor were compared with previous reports (Table 1).

Interference experiments were performed to investigate the selectivity of the proposed sensor towards detection of NO_2^- in presence of common ions such as urea acid (UA), ascorbic acid (AA) and glucose (Fig. 8a), NCE exhibited well defined amperometric response towards detection of 0.5 μM of nitrite, whereas no noteworthy amperometric responses were observed for the addition of 100, 40, and 100-fold excess of UA, AA, and glucose, respectively. But quick and stable response was observed again for the addition of 0.5 μM nitrite into the same PBS coexisting with the above said

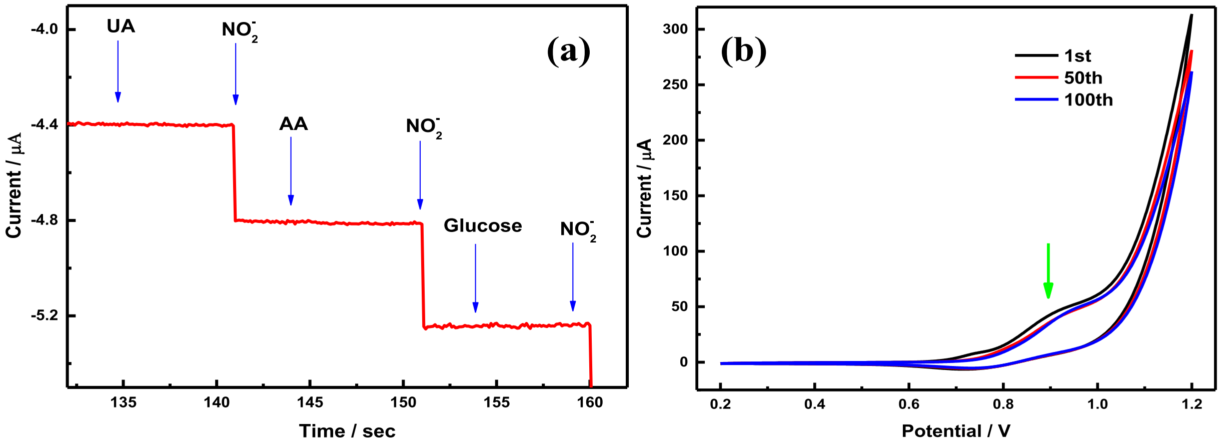

Fig. 8. (a) Amperometric response for the detection of 0.5 μM nitrite solution containing different interfering chemicals: 50 μM UA, 20 μM AA, 50 μM Glucose on NCE by applying a constant potential of 0.9 V. Each addition increases 0.5 μM nitrite. (b) Stability tests for NCE in 0.1 M PBS (pH 7.0) containing 10 μM nitrite.

interferences.

The stability of the NCE was also studied. The CV currents could be remained at constant values upon 100 continuous CV cycles at the potential range from 0.2 to 1.2 V in 0.1 M PBS (pH 7.0) with the scan rate of 50 mV s^{-1}. Fig. 8b shows that the current assigned to nitrite oxidation is 92.4% of the initial value after 100 cycles, thus suggesting good electrode stability owing to an efficient protection of Nafion on the NCE.

4. Conclusions

In summary, we fabricated a simple, urchin-like electrocatalyst with the utilization of the nickel and cobalt carbonate compound, which offers this novel nanomaterial promising application for sensitive detection of nitrite. The as-prepared electrode made up of NC and Nafion displayed good electrochemical response to nitrite with the linear range of 5–4000 μM and the detection limit of 0.002 μM. All of these results further confirmed that the NCE played a significant role in detection of nitrite. The successful application of nickel and cobalt carbonate compound indicates that modified electrode provide a new platform for designing sensors to determine nitrite sensitively and selectively. The fabricated nitrite biosensor also exhibited high sensitivity and good stability.

Acknowledgements

The financial supports from National Natural Science Foundation of China (61404075), China Postdoctoral Science Foundation (No.2016M601694) and Postdoctoral Science Foundation of Jiangsu Province (No.1601090B) are greatly acknowledged. S. Lu also thanked the Center of Analysis and Testing of Southeast University for its help in FESEM observation (Ying Zhang), BET operation (Zeming Wang).

References

[1] S. Peng, G. Jin, L. Li, K. Li, M. Srinivasan, S. Ramakrishna, J. Chen, Multi-functional electrospun nanofibres for advances in tissue regeneration, energy conversion & storage, and water treatment, Chem. Soc. Rev. 45 (2016) 1225–1241.

[2] C.A. Martínez-Huitle, M.A. Rodrigo, I. Sirés, O. Scialdone, Single and coupled electrochemical processes and reactors for the abatement of organic water pollutants: a critical review, Chem. Rev. 115 (2015) 13362–13407.

[3] Q. He, G. Zhou, F. Geng, W. Gao, W. Yu, Spatial distribution of aerosol hygroscopicity and its effect on PM 2.5 retrieval in East China, Atmos. Res. 170 (2016) 161–167.

[4] Q. Yin, J. Wang, M. Hu, H. Wong, Estimation of daily PM 2.5 concentration and its relationship with meteorological conditions in Beijing, J. Environ. Sci. 48 (2016) 161–168.

[5] Y. Wang, S. Hu, Applications of carbon nanotubes and graphene for electrochemical sensing of environmental pollutants, J. Nanosci. Nanotechnol. 16 (2016) 7852–7872.

[6] W. Lijinsky, E. Conrad, R. Van de Bogart, Carcinogenic nitrosamines formed by drug/nitrite interactions, Nature 239 (1972) 165–167.

[7] J.H. Seinfeld, S.N. Pandis, Atmospheric Chemistry and Physics: from Air Pollution to Climate Change, Wiley-Interscience, New York, 2006, pp. 761–818.

[8] K. Calfumán, M.J. Aguirre, P. Canete-Rosales, S. Bollo, R. Llusar, M. Isaacs, Electrocatalytic reduction of nitrite on tetraruthenated metalloporphyrins/Nafion glassy carbon modified electrode, Electrochimica Acta 56 (2011) 8484–8491.

[9] L. Fu, S. Yu, L. Thompson, A. Yu, Development of a novel nitrite electrochemical sensor by stepwise in situ formation of palladium and reduced graphene oxide nanocomposites, RSC Adv. 5 (2015) 40111–40116.

[10] J.O. Lundberg, E. Weitzberg, M.T. Gladwin, The nitrate–nitrite–nitric oxide pathway in physiology and therapeutics, Nat. Rev. Drug Discov. 7 (2008) 156–167.

[11] C. Lopez-Moreno, I.V. Perez, A.M. Urbano, Development and validation of an ionic chromatography method for the determination of nitrate, nitrite and chloride in meat, Food Chem. 194 (2016) 687–694.

[12] J. Wu, X. Wang, Y. Lin, Y. Zheng, J.-M. Lin, Peroxynitrous-acid-induced chemiluminescence detection of nitrite based on microfluidic chip, Talanta 154 (2016) 73–79.

[13] Z. Kalaycıoğlu, F.B. Erim, Simultaneous determination of nitrate and nitrite in fish products with improved sensitivity by sample stacking-capillary electrophoresis, Food Anal. Methods 9 (2016) 706–711.

[14] K.M. Miranda, M.G. Espey, D.A. Wink, A rapid, simple spectrophotometric method for simultaneous detection of nitrate and nitrite, Nitric Oxide 5 (2001) 62–71.

[15] J. Davis, M.J. Moorcroft, S.J. Wilkins, R.G. Compton, M.F. Cardosi, Electrochemical detection of nitrate and nitrite at a copper modified electrode, Analyst 125 (2000) 737–742.

[16] S. Radhakrishnan, K. Krishnamoorthy, C. Sekar, J. Wilson, S.J. Kim, A highly sensitive electrochemical sensor for nitrite detection based on Fe_2O_3 nanoparticles decorated reduced graphene oxide nanosheets, Appl. Catal. B Environ. 148 (2014) 22–28.

[17] H. Wu, S. Fan, W. Zhu, Z. Dai, X. Zou, Investigation of electrocatalytic pathway for hemoglobin toward nitric oxide by electrochemical approach based on protein controllable unfolding and in-situ reaction, Biosens. Bioelectron. 41 (2013) 589–594.

[18] J. Jiang, W. Fan, X. Du, Nitrite electrochemical biosensing based on coupled graphene and gold nanoparticles, Biosens. Bioelectron. 51 (2014) 343–348.

[19] Y.G. Guo, J.S. Hu, L.J. Wan, Nanostructured materials for electrochemical energy conversion and storage devices, Adv. Mater. 20 (2008) 2878–2887.

[20] J. Wang, Y. Fu, Y. Xu, J. Wu, J.-H. Tian, R. Yang, Hierarchical $NiCo_2O_4$ hollow nanospheres as high efficient bi-functional catalysts for oxygen reduction and evolution reactions, Int. J. Hydrog. Energy 41 (2016) 8847–8854.

[21] X. Lv, Y. Zhu, H. Jiang, X. Yang, Y. Liu, Y. Su, J. Huang, Y. Yao, C. Li, Hollow mesoporous $NiCo_2O_4$ nanocages as efficient electrocatalysts for oxygen evolution reaction, Dalton Trans. 44 (2015) 4148–4154.

[22] G. Gao, H.B. Wu, S. Ding, L.M. Liu, X.W. Lou, Hierarchical $NiCo_2O_4$ nanosheets grown on Ni nanofoam as high-performance electrodes for supercapacitors, Small 11 (2015) 804–808.

[23] X. Tong, S. Chen, C. Guo, X. Xia, X.Y. Guo, Mesoporous $NiCo_2O_4$ nanoplates on three-dimensional graphene foam as an efficient electrocatalyst for the oxygen reduction reaction, ACS Appl. Mater. Interfaces 8 (42) (2016) 28274–28282.

[24] G. Zhang, B.Y. Xia, X. Wang, Strongly coupled $NiCo_2O_4$-rGO hybrid nanosheets as a methanol-tolerant electrocatalyst for the oxygen reduction reaction, Adv. Mater. 26 (2014) 2408–2412.

[25] Y. Xiao, C. Hu, L. Qu, C. Hu, M. Cao, Three-dimensional macroporous $NiCo_2O_4$ sheets as a non-noble catalyst for efficient oxygen reduction reactions, Chem. A Eur. J. 19 (2013) 14271–14278.

[26] H.-P. Cong, S.-H. Yu, Shape control of cobalt carbonate particles by a hydrothermal process in a mixed solvent: an efficient precursor to nanoporous cobalt oxide architectures and their sensing property, Cryst. Growth Des. 9 (2008) 210–217.

[27] J. Xiao, S. Yang, Sequential crystallization of sea urchin-like bimetallic (Ni, Co) carbonate hydroxide and its morphology conserved conversion to porous $NiCo_2O_4$ spinel for pseudocapacitors, RSC Adv. 1 (2011) 588–595.

[28] C. Shang, S. Dong, S. Wang, D. Xiao, P. Han, X. Wang, L. Gu, G. Cui, Coaxial $Ni(_x)Co(_{2x})(OH)(_{6x})$/TiN nanotube arrays as supercapacitor electrodes, ACS Nano 7 (2013) 5430–5436.

[29] Q. Shi, Z. Chen, Z. Song, J. Li, J. Dong, Synthesis of ZIF-8 and ZIF-67 by steam-assisted conversion and an investigation of their tribological behaviors, Angew. Chem. Int. Ed. 50 (2011) 672–675.

[30] S. Brunauer, P.H. Emmett, E. Teller, Adsorption of gases in multimolecular layers, J. Am. Chem. Soc. 60 (1938) 309–319.

[31] J. Wu, R. Mi, S. Li, P. Guo, J. Mei, H. Liu, W.-M. Lau, L.-M. Liu, Hierarchical three-dimensional $NiCo_2O_4$ nanoneedle arrays supported on Ni foam for high-performance supercapacitors, RSC Adv. 5 (2015) 25304–25311.

[32] O. Brylev, M. Sarrazin, L. Roué, D. Bélanger, Nitrate and nitrite electrocatalytic reduction on Rh-modified pyrolytic graphite electrodes, Electrochimica Acta 52 (2007) 6237–6247.

[33] T. Wu, J. Li, L. Hou, C. Yuan, L. Yang, X. Zhang, Uniform urchin-like nickel cobaltite microspherical superstructures constructed by one-dimension nanowires and their application for electrochemical capacitors, Electrochimica Acta 81 (2012) 172–178.

[34] R. Guidelli, F. Pergola, G. Raspi, Voltammetric behavior of nitrite ion on platinum in neutral and weakly acidic media, Anal. Chem. 44 (1972) 745–755.

[35] P. Wang, Z. Mai, Z. Dai, Y. Li, X. Zou, Construction of Au nanoparticles on choline chloride modified glassy carbon electrode for sensitive detection of nitrite, Biosens. Bioelectron. 24 (2009) 3242–3247.

[36] J.-J. Feng, P.-P. Zhang, A.-J. Wang, Y. Zhang, W.-J. Dong, J.-R. Chen, One-pot hydrothermal synthesis of uniform β-MnO 2 nanorods for nitrite sensing, J. Colloid Interface Sci. 359 (2011) 1–8.

[37] S.-S. Li, Y.-Y. Hu, A.-J. Wang, X. Weng, J.-R. Chen, J.-J. Feng, Simple synthesis of worm-like Au-Pd nanostructures supported on reduced graphene oxide for highly sensitive detection of nitrite, Sens. Actuators B Chem. 208 (2015) 468–474.

[38] A. Afkhami, F. Soltani-Felehgari, T. Madrakian, H. Ghaedi, Surface decoration of multi-walled carbon nanotubes modified carbon paste electrode with gold nanoparticles for electro-oxidation and sensitive determination of nitrite, Biosens. Bioelectron. 51 (2014) 379–385.

[39] Z. Wang, F. Liao, T. Guo, S. Yang, C. Zeng, Synthesis of crystalline silver nanoplates and their application for detection of nitrite in foods, J. Electroanal. Chem. 664 (2012) 135–138.